



Measurement of laser shock peening induced residual stress by nanoindentation and comparison with XRD technique

A. Greco^a, E. Sgambitterra^{a,*}, M. Guagliano^b, F. Furgiuele^a

^a University of Calabria, Department of Mechanical, Energy and Management Engineering, Rende, CS, Italy

^b Politecnico di Milano, Department of Mechanical Engineering, Milano, Italy

ARTICLE INFO

Keywords:

Laser shock peening
Residual stress
Nanoindentation
Finite element method

ABSTRACT

Laser shock peening (LSP) is an innovative surface treatment technique successfully used to improve fatigue performance of metallic components. It is based on the application of high intensity laser and suitable overlays with the aim to generate high pressure shock waves on the surface of the mechanical part to be treated. Shock waves generate severe plastic deformations and, consequently, compressive residual stresses (RS). An accurate measurement of these latter is crucial for predicting the resistance of treated parts under service loads and to assess the effectiveness of LSP process.

In this paper, a non-destructive method, based on the nanoindentation technique and finite element analysis (FEA), was developed to measure the RS generated by LSP process on AA-7050-T451 samples. In particular, the methodology is based on the analysis of the nanoindentation peak load variation generated by the presence of residual stresses on a component. Obtained results were compared, for validation, with the measurements carried out by the most consolidated X-ray diffractometer (XRD) technique. The results showed a satisfactory agreement between the two techniques, revealing nanoindentation as a promising and reliable method for characterizing RS induced by LSP.

1. Introduction

Any mechanical component, made in a workmanlike way, assumes that the shape, the material properties, and the surface finishes are adequate for its specific application. However, the operating conditions are often different from the nominal ones as a consequence of non-predictable phenomena that can induce premature failure. For instance, one can consider vibrations, low cyclic forces and/or overloads that can trigger crack initiation and consequently induce fatigue failure. Even the working environment itself can represent an additional element of variability. In fact, the presence of machining dust, metal shavings, grease or dirt can make the working environment quite different from the nominal one. For this reason, in the technological development process, finishing methods of the machined surfaces were developed, with the aim to make the component less susceptible to not controllable conditions. For example, to guarantee corrosion protection of materials, special paints or metallic coatings are used. On the other hand, to prevent fatigue phenomena, surface treatments of the component can be done to strengthen the first layers [1].

In this field, among the different surface treatment technologies, one

of the most used is the shot peening. It is a cold mechanical working process which involves "shooting" metal balls (or other materials, depending on the component to be treated and the result to be obtained) which plastically deform the surface of the component. These deformations induce residual compressive stresses which help in protecting from fatigue phenomena.

Laser Shock Peening (LSP) is a relatively recent treatment technique (the first patents in this field date back to 1963), used, at the same way, to induce residual compressive stresses in metallic materials [2]. For some aspects it is quite similar to the standard shot peening. However, LSP involves high intensity laser and suitable overlays to generate high pressure shock waves on the surface of the part to be treated which cause intense plastic deformations and compressive residual stresses. These latter allow to prevent the propagation of cracks and increase the fatigue strength of the material [3–6].

LSP is a non-invasive process and can be used to improve the mechanical properties of components working in critical operating conditions in fields as aeronautics, automotive and biomedical. The technique offers many advantages, including the ability to improve the performance of parts without significantly changing their dimensions and

* Corresponding author.

E-mail address: emanuele.sgambitterra@unical.it (E. Sgambitterra).

<https://doi.org/10.1016/j.jmrt.2024.05.017>

Received 20 March 2024; Received in revised form 25 April 2024; Accepted 2 May 2024

Available online 3 May 2024

2238-7854/© 2024 The Authors. Published by Elsevier B.V. This is an open access article under the CC BY license (<http://creativecommons.org/licenses/by/4.0/>).

geometries, guarantying greater durability and reliability of the treated. In addition, compared to the classical shot peening technique, LSP generates a better surface finish after the treatment, according to the laser energy [7], and has the capability to generate residual compressive stresses at greater depth, in the order of 3–4 mm, compared to 0.5 mm of the shot peening, with most benefits in the fatigue resistance. In fact, induced residual stresses will combine with the service load by changing the nominal applied stress field [8,9]. Therefore, it is of great interest, especially for safety conditions, measure the residual stresses induced by the surface treatment.

This latter is generally not an easy task but in the last decades several methods were developed [10,11]. In particular, they can be classified as i) destructive/mechanical as the hole drilling, crack compliance, contouring and ii) non-destructive/physical as the X-Ray, photoelasticity, ultrasound, etc.

Beyond the semi-destructive methods, nanoindentation allows rapid, accurate and economic testing but its practical application is limited as it is a relatively young methodology that still needs improvements and validation by direct comparison with most consolidated techniques [12–15]. In fact, up to now, nanoindentation was widely used to investigate the mechanical properties, as hardness, Young's modulus, fracture toughness of small material volumes [16], as well as to determine damage mechanisms generated by static and fatigue loads [17]. For its practical application on the RS measurements, many efforts are still required. The basic idea is to measure the modification of the force-penetration response of a sample when it is affected by residual stresses, compared to a stress-free material and by the analysis of the nanoindentation outcomes it is possible to estimate the RS magnitude and sign [12,18,19].

To this aim, different parameters can be taken into account as the indentation contact area [20], the loading curvature [21], the indentation work [22] or the peak load [23]. In this latter case, in particular, it was shown that, when the maximum penetration depth is specified, compressive RS increases the peak load required to penetrate the sample whereas tensile RS decreases the peak load [23]. In the case of equal principal RS components (equi-biaxial RS) in the investigation plane, a standard indenter tip (i.e., Berkovich tip) is used to determine the peak load. Once the relation between RS and peak load is derived, numerically or experimentally, RS can be estimated [15]. For non-equi-biaxial RS, it is also necessary to use an indenter tip that is sensible to the orientation of the principal RS components in the indentation plane and to do multiple indentations. For this purpose, in a previous work by the authors [12] a modified Berkovich tip, that is obtained from the elongation of the classical Berkovich in one direction, has been proposed.

This work aims in exploiting this customized tip to measure the RS

field induced by LSP treatment on a sample made by AA7050-T7451 (main LSP parameters: pulse energy 5 J, pulse length 20 ns, pulse frequency 5 Hz, spot diameter 5 mm, offset 33%). To this aim, nano-indentation tests were carried out in depth control mode and the peak load was selected as the parameter for the RS estimation. In order to obtain a relation between RS and load variation with respect to the stress-free (blank) sample, finite element analysis (FEA) was also used. In this paper, the LSP-treated specimen is firstly analyzed with the classical Berkovich tip to determine an average value between the principal RS components (as if the RS field was equi-biaxial) and then the modified Berkovich tip is used to determine the non-equi-biaxial RS field. Obtained estimations were, finally, compared with the measurements carried out with a XR diffractometer. Results revealed satisfactory agreement.

2. Methodology

2.1. Equi-biaxial residual stress

The RS measurement methodology is based on the principle shown in Fig. 1. In particular, when a specimen is indented in depth control mode, i.e., specifying the maximum penetration depth, the recorded peak load depends on the magnitude and the sign of RS. In detail, as shown in Fig. 1a, naming L_{SF} the peak load required to penetrate the sample in stress-free conditions, one can observe that compressive RS increases the peak load, L_c , whereas tensile RS generates lower peak loads, L_t , than the stress-free conditions [15]. Furthermore, the load variation ΔL is dependent on the RS magnitude, as reported in Fig. 1b. Based on these considerations, a relation between equi-biaxial RS and the nano-indentation peak loads can be univocally determined. To this aim, numerical finite element indentations were carried out by simulating the nanoindentation process on samples under stress free conditions and under the effect of known mechanical applied stresses that simulates equi-biaxial RS. More details about the finite element simulations are reported in Section 3. Once the correlation between the peak loads and RS is known, one can use such information to estimate the presence of RS on a real mechanical part by simply doing indentations and measuring the peak load obtained on the LSP-treated sample L_{LSP} (i.e., under the effect of the applied stress) and compare it with the one obtained in stress-free conditions L_{SF} .

In addition, the relative load difference, dL , can be also obtained as follows:

$$dL = (L_{LSP} - L_{SF}) / L_{SF} \quad (1)$$

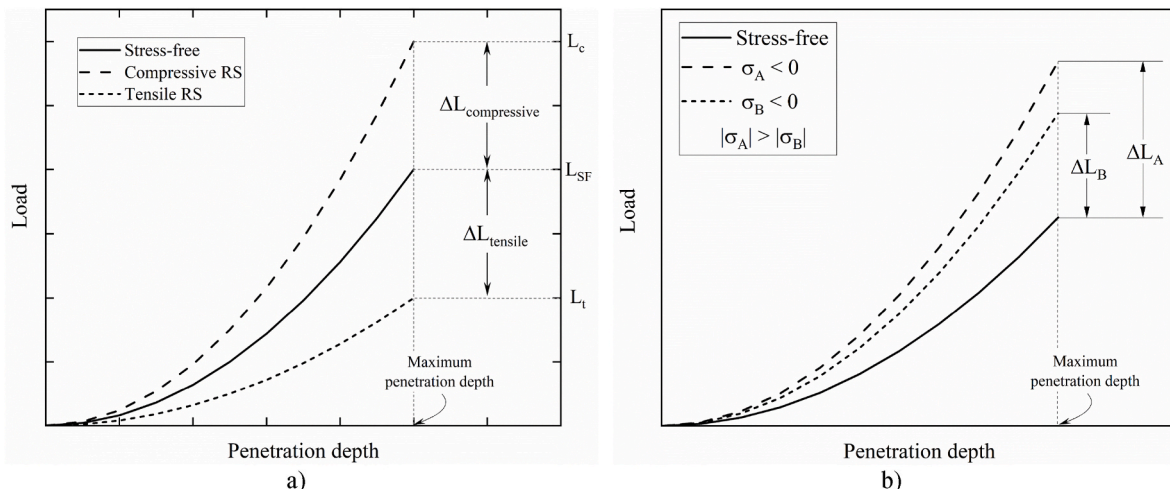


Fig. 1. Scheme of the residual stress (RS) effect on the nanoindentation curves: a) effect of the sign of RS; b) effect of the magnitude of RS.

2.2. Non-equi-biaxial residual stress

In the case of generically biaxial residual stress, the estimation of the RS field requires a great number of data the application of an indenter tip that is sensible to the orientation of principal RS components. The use of a standard axisymmetric nanoindenter tip, i.e., Berkovich tip see Fig. 2a, does not allow to measure the principal RS components by only exploiting the peak load recorded by the nanoindenter platform as this kind of tip cannot distinguish between the different orientation of the RS components. Consequently, in a previous work by the authors [12] it was successfully numerically investigated the use of a modified Berkovich tip, obtained from the elongation of the classical Berkovich tip in one direction, see Fig. 2b, for the measurement of non-equi-biaxial residual stresses.

In particular, the basic idea of the method was to exploit the change of the peak load as a function of sign, magnitude and also orientation of principal RS components in the indentation plane. Since the indenter tip is elongated in one direction, changing its orientation in the indentation plane results in a variation of the recorded peak load. In detail, if the direction of the principal RS components is known a priori, the unknowns are the two principal residual stress components in the indentation plane. Consequently, as schematically presented in Fig. 3, two indentations along the principal RS components directions are sufficient to fully determine the RS field exploiting a linear correlation between RS and peak load. The correlation coefficient, named $\gamma_{||}$ and γ_{\perp} , can be determined via Finite Element Analysis (FEA).

If the direction of the principal RS components is unknown, the unknowns are the two principal residual stress components as well as their orientation in the indentation plane. Consequently, three indentations, rotated by 45° relative to each other, are required. Fig. 4 summarize the main steps of this method; further details about this methodology are described in Ref. [12].

3. Finite element analyses

Two finite element models were implemented by the commercial code ABAQUS CAE (Dassault Systemes, 2020) to simulate the nanoindentation process in the case of equi-biaxial RS (Berk-FEM) and in the case of non-equi-biaxial RS (Mod-Berk-FEM). These models aim to mathematically relate RS and nanoindentation peak load variation, in both equi- and non-equi-biaxial RS cases.

Both finite element models are made by the specimen to indent and the nanoindenter tip. Because of the loading and geometrical symmetry, a quarter of the bodies was modelled in Berk-FEM whereas in Mod-Berk-FEM half parts are required. The specimen was modelled as a

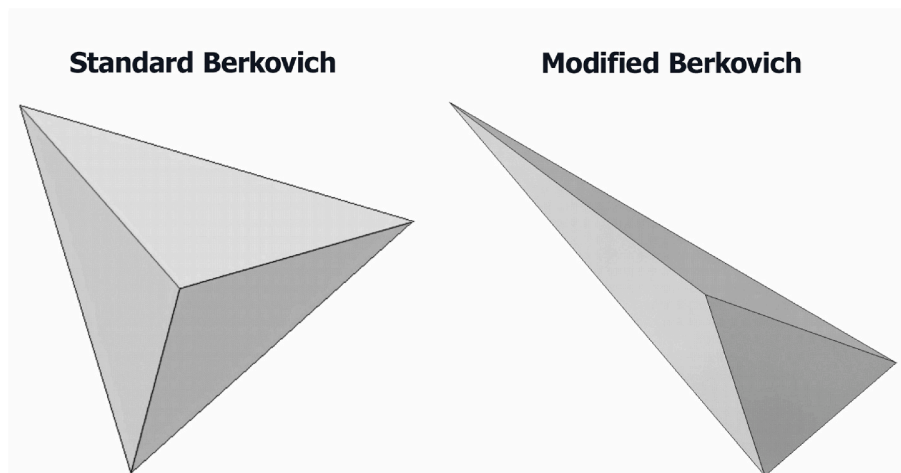


Fig. 2. Representation of nanoindenter tips: a) classical Berkovich tip; b) modified Berkovich tip, obtained from the elongation of the classical Berkovich tip.

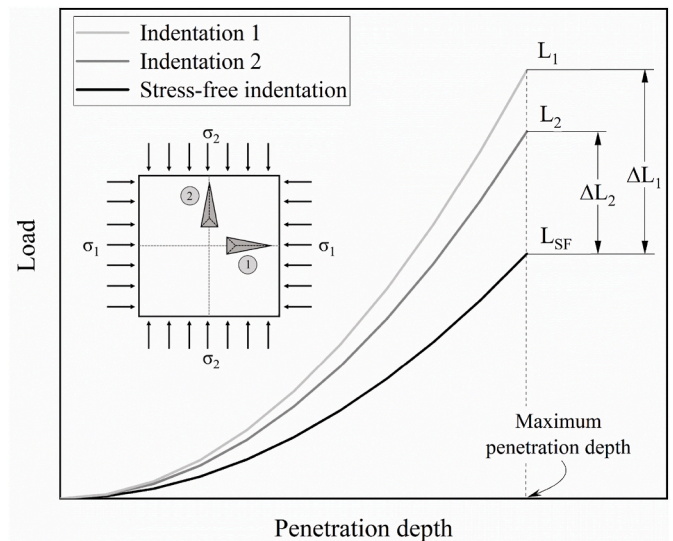


Fig. 3. Representation of the nanoindentation curves obtained using the modified Berkovich tip along the principal residual stress components directions in a biaxial compressive residual stress field ($\sigma_2 < \sigma_1 < 0$).

deformable part discretized in about 150000 C3D4 elements in Berk-FEM and in about 900000 C3D4 elements in Mod-Berk-FEM. The investigated material is the AA7050-T7451, and both the elastic and plastic domains were implemented to define the behaviour of the specimen. Fig. 5 presents the elastoplastic behaviour of the material and reports all the experimentally obtained parameters of interest.

The indenter tip is modelled as a discrete rigid part in both FEM models. In detail, in Berk-FEM, the Berkovich tip is modelled as an equivalent cone with an apex angle of 70.3° , without generating big simulation errors as demonstrated by Refs. [24,25], and meshed in about 18000 R3D4 elements. In Mod-Berk-FEM, the modified Berkovich tip is modelled in its real geometry and meshed in about 100000 R3D4 elements. Mesh-sensitivity analysis results in a refinement of the mesh near the contact zone. With the aim of avoiding boundary effects, the overall sizes of the model are 2 orders of magnitude greater than the contact zone dimensions. Fig. 6 presents the FE assemblies with a magnified highlight of the sample penetration zone, Berk-FEM in Fig. 6a and Mod-Berk-FEM in Fig. 6b.

The interaction between bodies is modelled as a master-slave contact with no friction, since it is totally negligible for the peak load investigation [12,24]. Uniformly distributed pressure loads of different

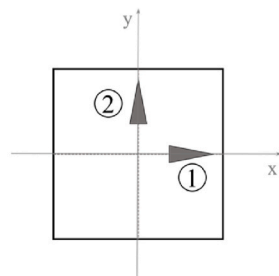
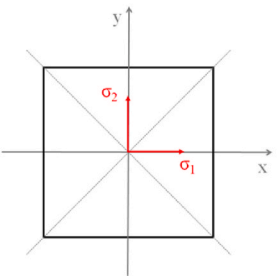
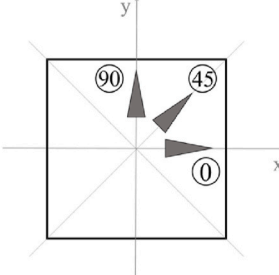
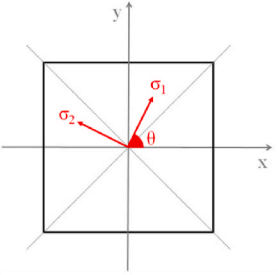
CASE	MEASUREMENTS	RESULTS	ANALYTICAL MODEL
Known principal directions			$\Delta L_1 = \gamma_{\parallel} \cdot \sigma_1 + \gamma_{\perp} \cdot \sigma_2$ $\Delta L_2 = \gamma_{\perp} \cdot \sigma_1 + \gamma_{\parallel} \cdot \sigma_2$
Unknown principal directions			$\begin{bmatrix} \Delta L_0 \\ \Delta L_{45} \\ \Delta L_{90} \end{bmatrix} = \begin{bmatrix} \gamma_{\parallel} & 0 & \gamma_{\perp} \\ \gamma_{\perp} & \gamma_{\parallel} - \gamma_{\perp} & \gamma_{\perp} \\ \gamma_{\perp} & 0 & \gamma_{\parallel} \end{bmatrix} \cdot \begin{bmatrix} \sigma_0 \\ \sigma_{45} \\ \sigma_{90} \end{bmatrix}$ $\begin{bmatrix} \sigma_0 \\ \sigma_{45} \\ \sigma_{90} \end{bmatrix} \xrightarrow{\text{Mohr's circle}} \begin{bmatrix} \sigma_1 \\ \sigma_2 \\ \theta \end{bmatrix}$

Fig. 4. Scheme of the RS measurement methodology using the modified Berkovich nanoindenter tip. For known principal RS components directions, the principal stress σ_1 and σ_2 are linearly related to the peak load variations ΔL_1 and ΔL_2 derived from indentation 1 and 2, and through the conversion factors γ_{\parallel} and γ_{\perp} . In the case of unknown principal directions, the stress components σ_0 , σ_{45} and σ_{90} are linearly derived from the peak load variations ΔL_0 , ΔL_{45} and ΔL_{90} from indentations oriented at 0° , 45° and 90° from a reference direction. Once σ_0 , σ_{45} and σ_{90} are known, the Mohr's circle can be used to determine σ_1 and σ_2 and their inclination θ respect to the reference direction.

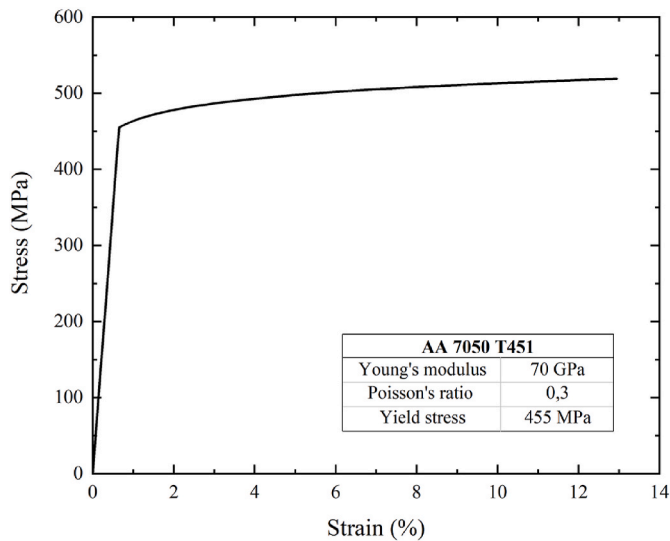


Fig. 5. Stress-strain curve of AA 7050 T451 implemented in the FEM models.

magnitude are used to simulate residual stresses. In detail, in the case of Berk-FEM, the magnitude of the mechanically applied pressures (that simulates RS) is equal in x- and z-direction of Fig. 6a in order to reproduce equi-biaxial RS. Instead, in the case of Mod-Berk-FEM, the magnitude of the mechanically applied pressures (that simulates RS) is not equal in x- and z-direction of Fig. 6b in order to reproduce non-equi-biaxial RS.

A maximum penetration depth of 2000 nm was simulated in both Berk-FEM and Mod-Berk-FEM.

4. Experiments

4.1. Nanoindentation tests

The nanoindentation platform NHT2 (CSM Instruments, Switzerland), with a load capacity of 500 mN, has been used for testing, at room temperature. In particular, nanoindentation tests were carried out in depth control mode on both stress-free and LSP-treated AA7050-T7451 samples, using both classical and modified Berkovich tips, up to a specified maximum penetration depth. Each measurement was repeated 30 times for statistical purposes through matrices of 5x6 indentations; a proper distance between the imprints, along the horizontal and vertical directions, was set to avoid interaction and interference effects among measurements: 100 μm for the Berkovich tip and 200 μm for the modified Berkovich tip.

Before the experiments, both stress-free and LSP-treated samples were cold mounted and mechanically polished by diamond compound (0.25 μm) in order to reduce the initial roughness of the samples and get mirror like surface. Particular attention was done for the LSP sample as the laser treatment generates relatively big sized dents. In this case, in fact, the average surface roughness of the LSP-treated sample was $R_a = 1.11 \mu\text{m}$ and the maximum height of the roughness was $R_t = 3.44 \mu\text{m}$. Please consider that the polishing treatment with this small-sized diamond does not influence the existing residual stress [26].

For the Berkovich tips, different maximum penetration depths were selected, from 1000 to 3500 nm with a step of 500 nm, to investigate the effect of this parameter (scale effect) on the peak load measurement. For each penetration depth, the maximum load was recorded to be used in equation (1).

For the modified Berkovich tips, the maximum penetration depth was set to 2000 nm. When the stress-free sample is indented, the direction of the indenter does not influence the measurement. For the LSP-treated sample, three matrices of indentations, at 2000 nm of maximum penetration depth, have been collected to determine ΔL_0 , ΔL_{45} , and ΔL_{90} , as in Fig. 4.

Fig. 7 shows the nanoindenter platform (Fig. 7a) and the residual

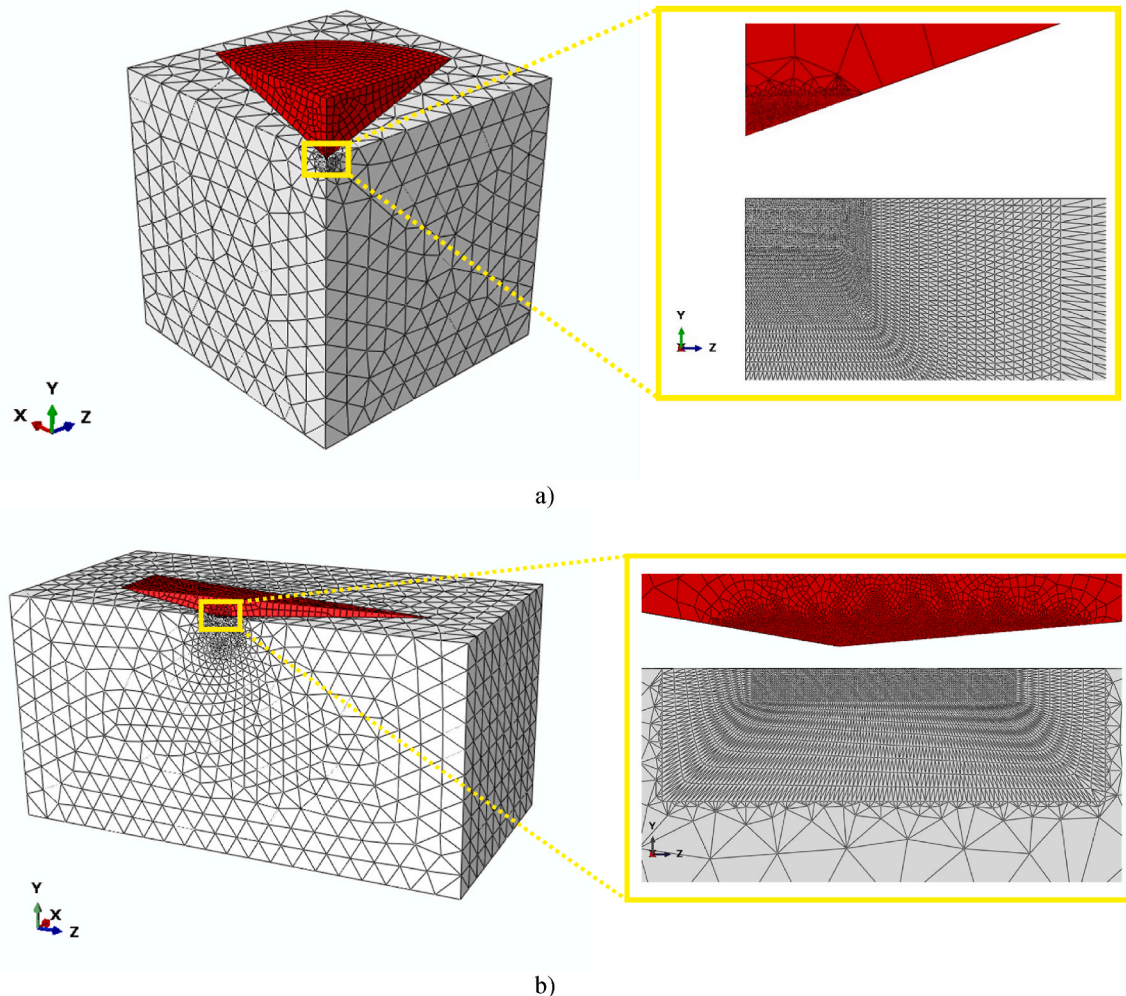


Fig. 6. Nanoindentation FE assemblies with a magnified highlight of the sample penetration zone: a) Berk-FEM; b) Mod-Berk-FEM.

imprints of the indentations carried out with a maximum penetration depth of 2000 nm using the classical Berkovich tip (Fig. 7b) and the modified Berkovich tip (Fig. 7c).

4.2. XRD measurements

The surface residual stresses induced by LSP were also measured with an X-ray diffractometer with the aim to compare these results with the ones obtained with the nanoindentation method and assess the accuracy of this latter approach.

XRD residual stress analysis was carried out by using a XStress 3000 G2/G2R X-ray Stress Analyzer (radiation Cr-K α , irradiated area of 4 mm diameter, $\sin^2\psi$ method and diffraction angle (2θ) $\sim 139^\circ$ scanned between $\psi = 45^\circ$ and $\psi = -45^\circ$), corresponding to 311-reflex, scanned with a total of 7 tilts in the range of -45° along three rotations of 0° , 45° and 90° , with constant step size of 0.028° . The measurement was executed in agreement with the NPL good practice recommendations [27].

Two different points were investigated to assess the uniformity of the residual stress state. In Fig. 8 a picture of the sample positioned in the XR diffractometer is shown: the two points where the measurements were done are shown. The measurements are referred to a depth of 5.5 μm from the surface.

5. Results and discussion

Fig. 9 report the nanoindentation curves obtained for different maximum penetration depths for the stress-free sample (Fig. 9a) and the LSP-treated sample (Fig. 9b) using the Berkovich indenter. Please consider that each curve represents the average data of the 30 indentations carried out for each maximum penetration depth. The overlapping of the curves, in the loading path, demonstrates the accuracy and repeatability of the experiments. Fig. 9c shows a comparison between the peak load obtained for the stress-free and the LSP-treated sample for the different maximum penetration depths. As LSP induces compressive RS, the maximum load for the LSP-treated sample is greater than the stress-free case, as previously discussed and reported in Fig. 1. Fig. 9d shows the relative load difference dL , calculated using equation (1) and expressed in percentage form. Results revealed slight differences between the different maximum penetration depths and an average relative load difference close to 9.4%. Obviously, RS magnitude in the LSP-treated sample depends on depth. However, the percentage peak load variations, for the penetration depth ranging from 1000 nm to 3500 nm, slightly vary resulting in an average value of 9.4%. Thus, no significant RS changes occur in this interval (1000–3500 nm). This can be justified as LSP-induced RS profile beneath the surface develops for penetration in the order of millimeter and can be considered almost constant in the penetration depth range 1000–3500 nm and the corresponding Berkovich process zone (≈ 15 times the penetration depth),

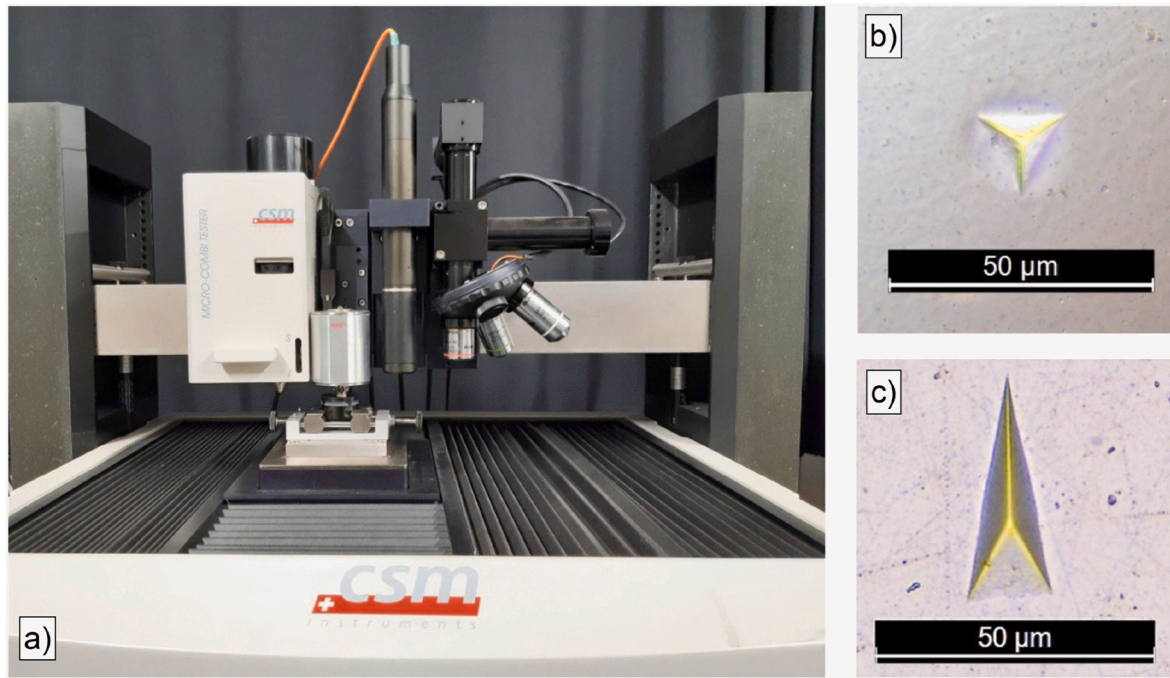


Fig. 7. Nanoindenter tests: a) NHT2 platform; b) residual imprints from Berkovich indentations; c) residual imprints from modified Berkovich indentations.

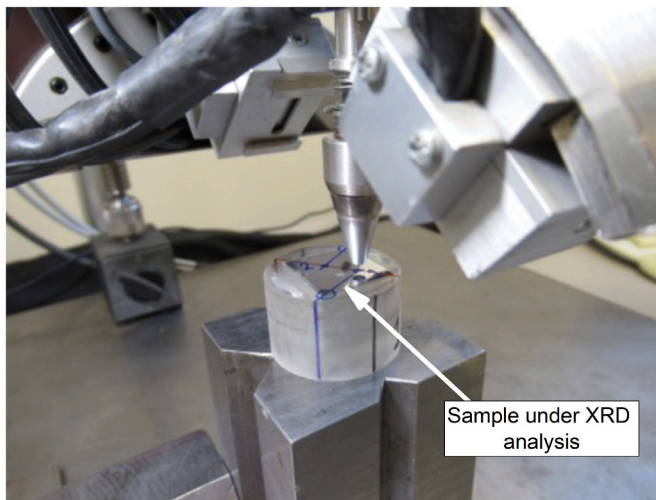


Fig. 8. The AA-7050-T451 sample positioned at the XR diffractometer. Points 1 and 2 are the locations where the residual stresses have been measured.

that is extremely reduced compared to the zone affected by LSP. For such reason, a maximum depth of 2000 nm was selected in order to do not overtake the load capacity of the nanoindenter platform and to guarantee a process zone beneath the indenter tip sufficiently big to interest a sufficient number of material grains and do not have crystallographic influence on the nanoindentation response.

Fig. 10a reports a comparison between the loading portion of the numerical and experimental nanoindentation curves obtained for the stress-free specimen when it is indented up to a maximum penetration depth of 2000 nm using the classical Berkovich tip. Results show good agreement between data revealing the accuracy of the implemented Berk-FEM.

After the validation, Berk-FEM was used to investigate the effect of equi-biaxial residual stress field on the peak load recorded during the nanoindentation process. Different equi-biaxial RS fields were applied over the Berk-FEM sample to derive a relation between the relative peak

load difference dL (see equation (1)) and the magnitude of the equi-biaxial RS field. **Fig. 10b** reports the graphical relation between the investigated values. In detail, σ_Y is the yield stress of the material, i.e., 455 MPa (see **Fig. 5**), and σ_R is the magnitude of the FEM-simulated RS principal components. Residual stresses involved in the analysis ranges from a ratio σ_R/σ_Y of -1.0 to 1.0 , since RS cannot overcome the yield stress of the material. The relationship between dL and the ratio σ_R/σ_Y is not linear and the effect of tensile RS on the peak load is higher than the compressive RS.

Based on the observations reported in **Fig. 9d**, i.e., a relative load difference of 9.4%, and according to the graphical relation reported in **Fig. 10b**, one can conclude that the assumed equi-biaxial RS field that LSP induces into the sample is a compressive stress field with a magnitude of $\sigma_R = 194 \pm 31$ MPa. It is important to point out that, even though the RS field inside the sample is not equi-biaxial, the use of the classical Berkovich tip allows to get an average value between the two RS principal components.

Fig. 11a reports a comparison between the loading portion of the numerical and experimental nanoindentation curves obtained for the stress-free specimen when it is indented with a maximum penetration depth of 2000 nm using the modified Berkovich tip. Results show very good agreement between data revealing the accuracy of the implemented finite element model Mod-Berk-FEM.

Fig. 11b shows the peak load value recorded for the blank specimen and for the LSP-treated sample positioned at 0° , 45° and 90° from a reference direction, with the modified Berkovich tip. The reference direction is assumed coincident with an edge of the sample. Obviously, since LSP treatment induce compressive RS, the peak value for the LSP-treated sample is greater than the one for the blank specimen, as similarly discussed in **Fig. 9c** for the classical Berkovich tip. It can be also observed in **Fig. 11a** that the rotation of the LSP-treated sample does not strongly affect the peak load value. This latter point is an indication that the principal RS components do not differ much from each other.

Different non-equi-biaxial RS fields were applied over the Mod-Berk-FEM sample to derive the calibration coefficients $\gamma_{||}$ and γ_{\perp} that relate RS and peak load variation, as synthetize in **Fig. 4**. **Table 1** reports the peak load values L_1 and L_2 obtained from Mod-Berk-FEM for different value of principal RS components σ_1 and σ_2 , see **Fig. 3**. The investigation is

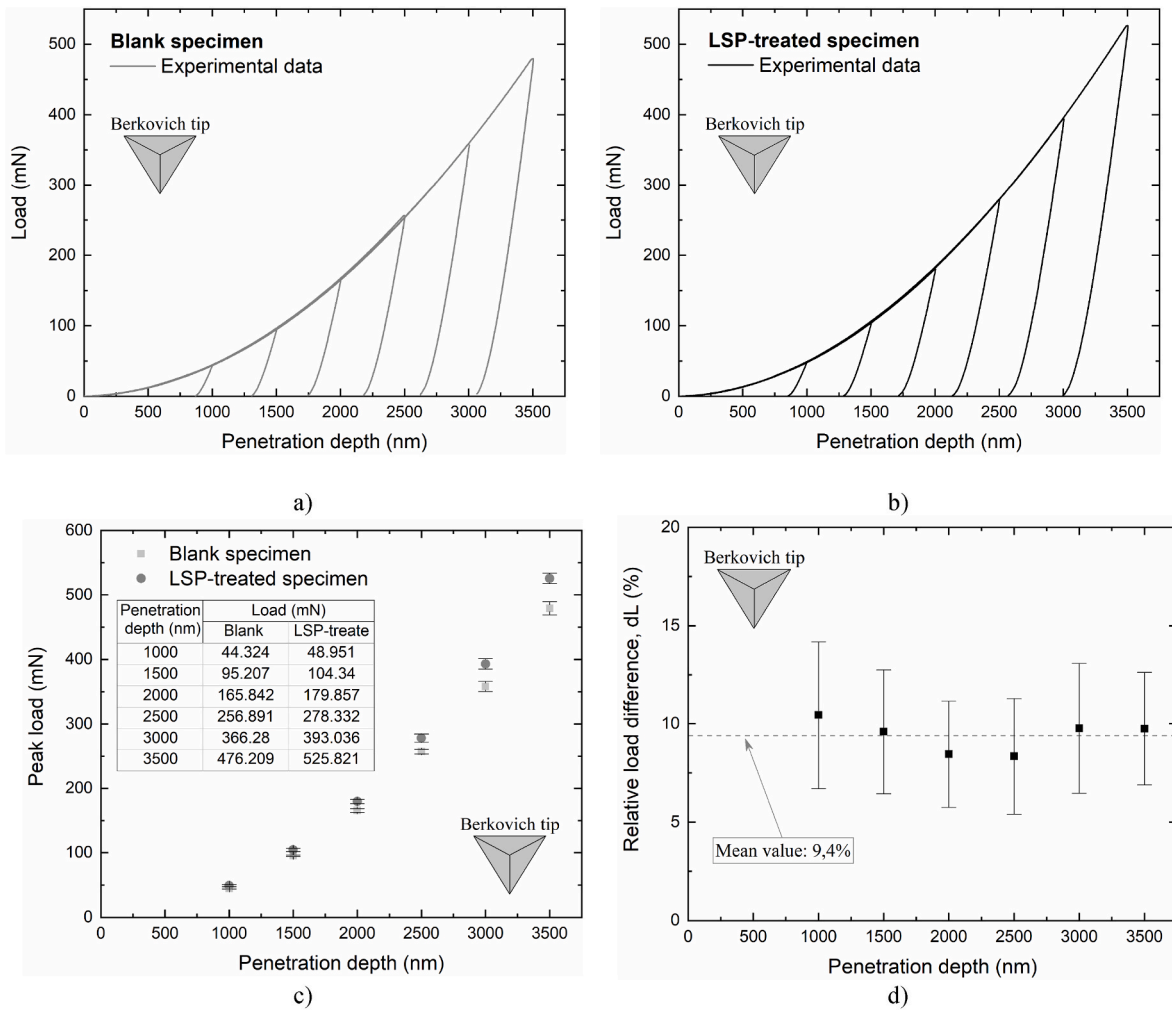


Fig. 9. Nanoindentation experimental data obtained for different penetration depths using Berkovich indenter. a) nanoindentation curves for blank specimen; b) nanoindentation curves for LSP-treated specimen; c) peak load recorded for blank and LSP-treated specimens for various penetration depths; d) relative load difference for LSP-treated specimen with respect to the blank specimen for various penetration depths.

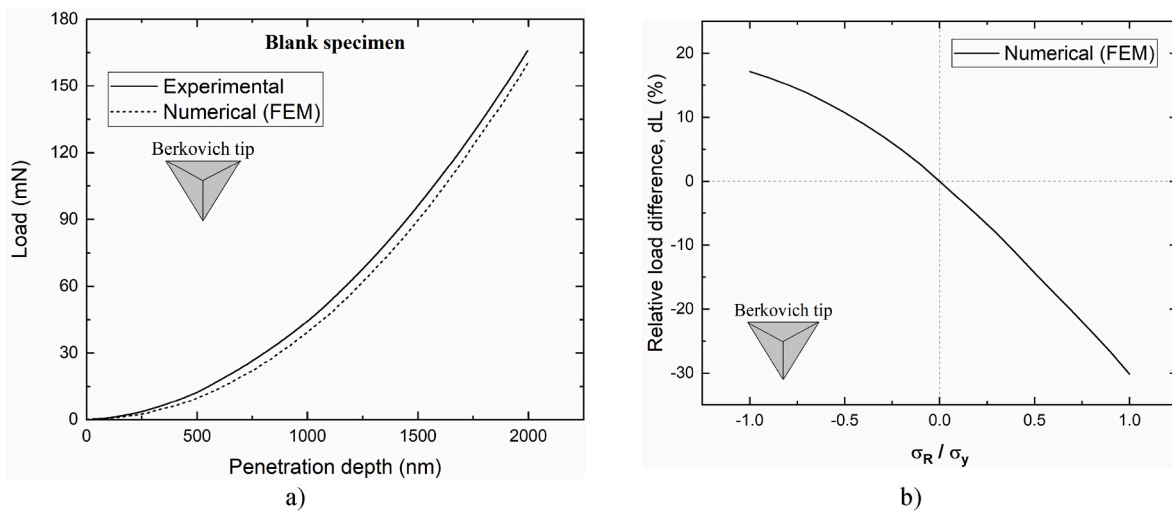


Fig. 10. FEA results for the classical Berkovich tip (Berk-FEM): a) loading portion of the nanoindentation curves obtained from FEA (dot-line) and from experiments (solid line) for a fixed maximum penetration depth of 2000 nm of the Al 7050 T451 blank sample using Berkovich indenter; b) relation between the equi-biaxial residual stress field and the percentage relative load difference recorded from Berk-FEM simulations.

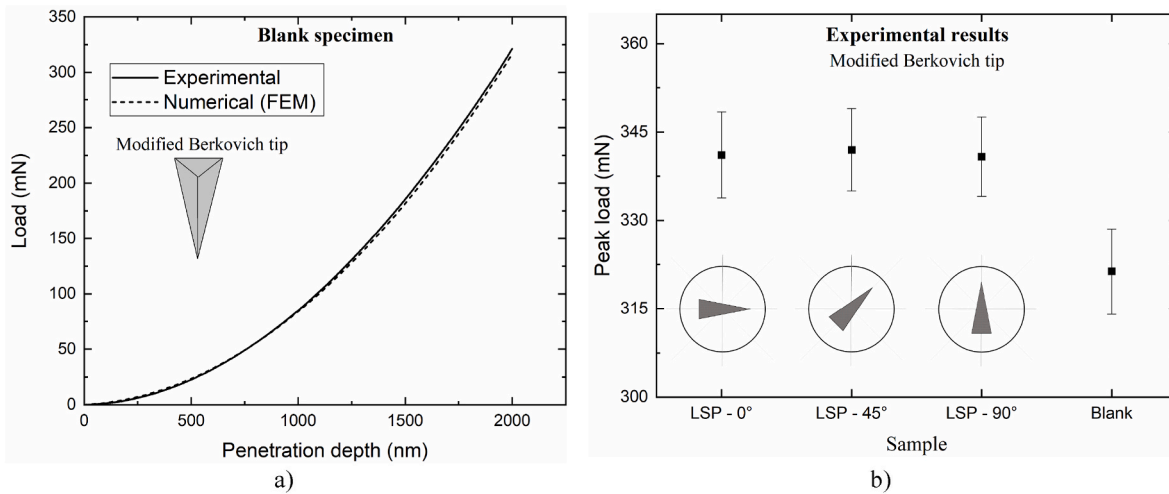


Fig. 11. a) peak load value recorded for the blank specimen and for the LSP-treated sample positioned at 0°, 45° and 90° from a reference direction using the Modified Berkovich tip; b) loading portion of the nanoindentation curves obtained from FEA (dot-line) and from experiments (solid line) for a fixed maximum penetration depth of 2000 nm of the Al 7050 T451 blank sample using modified Berkovich indenter.

Table 1

Peak load values L_1 and L_2 obtained from Mod-Berk-FEM for different value of principal RS components σ_1 and σ_2 . The RS components are expressed as a ratio of the yield stress σ_y of the material.

σ_1/σ_y	σ_2/σ_y	L_1 [mN]	L_2 [mN]
0.00	0.00	316.5	316.5
0.00	-0.25	325.7	320.1
0.00	-0.50	335.1	325.4
0.00	-0.75	339.9	326.6
0.00	-1.00	343.6	327.9
-0.25	-0.25	333.2	333.2
-0.25	-0.50	340.1	336.2
-0.25	-0.75	345.7	338.5
-0.25	-1.00	349.6	339.3
-0.50	-0.50	344.1	344.1
-0.50	-0.75	349.8	346.4
-0.50	-1.00	353.9	347.5
-0.75	-0.75	352.4	352.4
-0.75	-0.75	357.1	354.3
-1.00	-1.00	358.8	358.8

restricted to compressive RS field since the LSP-induced RS on the surface and sub-surface of the sample are compressive. Consequently, the ratios σ_1/σ_y and σ_2/σ_y ranges from 0.00 to -1.00.

Exploiting the values reported in Table 1 and through some mathematical steps accurately clarified in Ref. [12], it results for the simulated compressive RS that $\gamma_{\parallel} = -0.0339$ and $\gamma_{\perp} = -0.0684$. Combining these FEA-derived coefficients γ_{\parallel} and γ_{\perp} and the experimental peak load values represented in Fig. 11a (i.e., $L_{SF} = 321.31$ mN, $L_0 = 341.11$ mN, $L_{45} = 341.98$ mN, $L_{90} = 340.81$ mN) following the equations reported in Fig. 4 for the case of unknown principal RS directions, one can obtained that: $\sigma_1 = -162.1 \pm 39$ MPa; $\sigma_2 = -222.0 \pm 43$ MPa and $\vartheta = 40.8^\circ \pm 21^\circ$.

It can be simply observed that the RS value σ_R obtained using the classical Berkovich tip is exactly positioned between σ_1 and σ_2 obtained with the modified Berkovich tip, as expected.

Please notice that the proposed methodology is only based on the recording of the peak load by the nanoindentation platform. The pile-up formation is certainly influenced by RS but it cannot affect RS measurement since the plastic flow of the material and its accumulation around the tip is modelled in the FEA and since the method relies only on the peak load experimental measures.

Table 2 reports the XRD results of the residual stresses along the direction 0°, 45° and 90° as well as the principal residual stresses at

Table 2

Residual stresses measured by using the XRD technique (direction 0° and 90° are the direction of the diagonals of the sample, phi is the rotation of the principal directions with respect of the diagonals).

Position	σ_0 [MPa]	σ_{45} [MPa]	σ_{90} [MPa]	σ_1 [MPa]	σ_2 [MPa]	ϑ_{XRD} [°]
1	-201 ± 14	-200 ± 22	-180 ± 12	-176 ± 15	-205 ± 15	69°
	-203 ± 13	-166 ± 15	-158 ± 17	-154 ± 14	-208 ± 14	73°

points 1 and 2. It is important to point out that direction 0° and 90° are the direction of the diagonals of the sample and, ϑ_{XRD} is the rotation of the principal directions with respect of the diagonals. Consequently, ϑ obtained using nanoindentation can be expressed as $\vartheta = \vartheta_{XRD} - 45^\circ$.

The limited deviation (max 22 MPa with respect of 200 MPa) allows to say that the accuracy of the measurement is satisfactory and that the XR diffraction peaks are well aligned with respect of the $\sin^2\psi$ values.

The results show an almost equi-biaxial residual stress state, as previously assumed for the nanoindentation-based approach, with the stress components that show a limited variation in the three different direction and the principal stresses obviously aligned with these values.

Concerning the omogeneity of the LSP residual stresses on the treated surface, the values measured at points 1 and 2 show a more pronounced compression at point 2. However, the difference can be justified with the nature of the LSP process that is based on a pulsed laser shock, thus with possible limited variation from point to point.

If the XRD residual stress values are compared with the ones obtained by the hybrid method proposed in the present paper, the agreement is more than satisfactory. In fact, the hybrid FEM-experimental method results, both for the classical and the modified Berkovich nanoindenter tip, well agree with the one obtained using XRD method.

It is important to specify that the nanoindentation tests were carried out up to a maximum penetration depth of 2000 nm but, according with the FEAs, the process zone involved in the experiment is deeper. Consequently, the depth of 5.5 μm has been selected to compare the nanoindentation-based approach results with XRD measurements.

Finally, it is important to point out that the FEA were done by modelling the Al substrate with its untreated mechanical behavior. As well known, LSP treatment induces work-hardening near the surface material modifying its properties. Several research [28–32] demonstrated that strain hardening depends firstly on the material under

investigation as well as on the main LSP setting parameters. For the specific aluminum alloy, here analyzed, and the selected process parameter, the hardening effect on the RS estimation results minor. In fact, further numerical studies were done by modelling a harder material considering a 20% increase of tensile and yield stresses. Even in this extreme condition, the peak load for the stress-free specimen increases of about 5% and the RS percentage peak load variations remained almost identical.

Therefore, based on the literature studies [28–32] and on previous observations one can state that neglecting the material work-hardening, for the specific case under investigation, do not impact the research results.

6. Conclusions

In this paper, nanoindentation is used as a non-destructive technique to measure the biaxial RS field induced by the LSP process on an AA 7050 T451 sample. The measurements were carried out by combining the experimental nanoindentation outcomes with the FEM analysis. In detail, the variation of the peak load required to penetrate the sample until a maximum penetration depth varies with RS and, consequently, a relation between biaxial RS and relative load difference was established by FEA. The experimentally recorded relative load difference was compared to FEA results and the magnitude of the RS field was measured. Firstly, the classical Berkovich tip was used to determine an average value between the principal RS components. Then, a modified Berkovich tip, obtained from the elongation of the classical Berkovich in one direction, was exploited to fully determine the biaxial RS field induced by LSP in the sample.

The main outcomes of this research can be summarized as:

- No scale effect is registered for the percentage relative load difference as it is not dependent on the penetration depth. Consequently, the RS measurement is not affected by the selected maximum penetration depth;
- FEM well represents the nanoindentation process since the maximum error recorded between the FEA and the experimental peak load is less than 2.5%. The slight differences can be attributed to the material model used for simulation or to slight inaccuracy of the nanoindentation process. This error is however negligible;
- The relation between RS and the relative load difference is not linear and that tensile RS has a greater effect, as confirmed by literature [12,19].
- The comparison between the residual stresses obtained with the proposed hybrid method based on nanoindentation and the ones obtained with the most consolidated XRD technique is more than satisfactory and confirms the accuracy of the proposed method. Furthermore, the predicted RS field induced by LSP on the sample is totally in agreement with the literature [33]. Consequently, this work validates the proposed methodology for the RS measurement, both for equi-biaxial than for non-equi-biaxial RS field.
- The use of classical Berkovich tip instead of the modified one allows to rapidly obtain the value of the RS field in the sample. In fact, if the RS field is equi-biaxial the information obtained through the Berkovich tip is complete. Differently, for non-equi-biaxial RS field, only an average value between the principal RS components can be measured. In this latter case, even though the measure is not complete, it can be very useful adopting this approach to approximately determine the RS value in a rapid and economical way since only one indentation matrix is required for the treated sample and no modified indenter tip are required. Instead, the use of the customized modified Berkovich tip is more expensive in terms of time (three matrices of indentations are needed) and cost (the nanoindenter tip is not yet commercially available) but allows to fully determine the biaxial RS field in the sample.

In conclusion, the nanoindentation technique combined with FEM analysis allows to accurately measure the biaxial RS induced by LSP process and, more generally, any biaxial RS field in any sample.

Declaration of competing interest

The authors declare that they have no known competing financial interests or personal relationships that could have appeared to influence the work reported in this paper.

Acknowledgments

Nanoindentation experiments were carried out in the “MaTeRiA Laboratory” (University of Calabria), funded with “Pon Ricerca e Competitività 2007/2013”.

References

- [1] Scholtes B, Voehringer O. Mechanical surface treatment. In: Encyclopedia of materials: science and technology. Elsevier; 2001. p. 5253–61. <https://doi.org/10.1016/B0-08-043152-6/00916-5>.
- [2] Torres M. An evaluation of shot peening, residual stress and stress relaxation on the fatigue life of AISI 4340 steel. *Int J Fatig* 2002;24:877–86. [https://doi.org/10.1016/S0142-1123\(01\)00205-5](https://doi.org/10.1016/S0142-1123(01)00205-5).
- [3] Montross C. Laser shock processing and its effects on microstructure and properties of metal alloys: a review. *Int J Fatig* 2002;24:1021–36. [https://doi.org/10.1016/S0142-1123\(02\)00022-1](https://doi.org/10.1016/S0142-1123(02)00022-1).
- [4] Hereñú S, Strubbia R, Rubio-González C, Spadaro L, Bolmaro R, Gomez-Rosas G. High cycle fatigue life improvement of superferritic stainless steel by laser shock peening without coating. *Opt Laser Technol* 2022;152:108083. <https://doi.org/10.1016/j.optlastec.2022.108083>.
- [5] Dwivedi PK, Vinjamuri R, Rai AK, Ganesh P, Ranganathan K, Bindra KS, et al. Effect of laser shock peening on ratcheting strain accumulation, fatigue life and bulk texture evolution in HSLA steel. *Int J Fatig* 2022;163:107033. <https://doi.org/10.1016/j.ijfatigue.2022.107033>.
- [6] Guan L, Ye Z, Zhong J, Li Y, Zhang Y. Enhancement of corrosion resistance of 304L stainless steel treated by massive laser shock peening. *Opt Laser Technol* 2022;154:108319. <https://doi.org/10.1016/j.optlastec.2022.108319>.
- [7] Rodopoulos CA, Romero JS, Curtis SA, de los Rios ER, Peyre DP. Effect of controlled shot peening and laser shock peening on the fatigue performance of 2024-T351 aluminum alloy. *J Mater Eng Perform* 2003;12:414–9. <https://doi.org/10.1361/105994903770342944>.
- [8] Tabatabaeian A, Ghasemi AR, Shokrieh MM, Marzbanrad B, Baraheni M, Fotouhi M. Residual stress in Engineering materials: a review. *Adv Eng Mater* 2022; 24. <https://doi.org/10.1002/adem.202100786>.
- [9] James MN. Residual stress influences on structural reliability. *Eng Fail Anal* 2011; 18:1909–20. <https://doi.org/10.1016/j.engfailanal.2011.06.005>.
- [10] Guo J, Fu H, Pan B, Kang R. Recent progress of residual stress measurement methods: a review. *Chin J Aeronaut* 2021;34:54–78. <https://doi.org/10.1016/j.cja.2019.10.010>.
- [11] Huang X, Liu Z, Xie H. Recent progress in residual stress measurement techniques. *Acta Mech Solida Sin* 2013;26:570–83. [https://doi.org/10.1016/S0894-9166\(14\)60002-1](https://doi.org/10.1016/S0894-9166(14)60002-1).
- [12] Greco A, Sgambitterra E, Furguiele F. A new methodology for measuring residual stress using a modified Berkovich nano-indenter. *Int J Mech Sci* 2021;207:106662. <https://doi.org/10.1016/j.ijmecsci.2021.106662>.
- [13] Moharrami R, Sanayei M. Developing a method in measuring residual stress on steel alloys by instrumented indentation technique. *Measurement* 2020;158:107718. <https://doi.org/10.1016/j.measurement.2020.107718>.
- [14] Peng G, Xu F, Chen J, Wang H, Hu J, Zhang T. Evaluation of non-Equi-biaxial residual stresses in metallic materials via instrumented spherical indentation. *Metals* 2020;10:440. <https://doi.org/10.3390/met10040440>.
- [15] Greco A, Sgambitterra E, Furguiele F, Furfari D. A novel method to measure equi-biaxial residual stress by nanoindentation. *Exp Mech* 2023. <https://doi.org/10.1007/s11340-023-01001-5>.
- [16] Pharr GM, Oliver WC. Nanoindentation of silver-relations between hardness and dislocation structure. *J Mater Res* 1989;4:94–101. <https://doi.org/10.1557/JMR.1989.0094>.
- [17] Furguiele F, Greco A, Magarò P, Sgambitterra E. Analysis of the local functional evolution in NiTi shape memory alloys by multicycle nanoindentations. *Shap. Mem. Superelasticity* 2023. <https://doi.org/10.1007/s40830-023-00420-6>.
- [18] Moharrami R, Sanayei M. Improvement of indentation technique for measuring general biaxial residual stresses in austenitic steels. *Precis Eng* 2020;64:220–7. <https://doi.org/10.1016/j.precisioneng.2020.04.011>.
- [19] Sakharova NA, Prates PA, Oliveira MC, Fernandes JV, Antunes JM. A simple method for estimation of residual stresses by depth-sensing indentation. *Strain* 2012;48:75–87. <https://doi.org/10.1111/j.1475-1305.2010.00800.x>.
- [20] Suresh S, Giannakopoulos AE. A new method for estimating residual stresses by instrumented sharp indentation. *Acta Mater* 1998;46:5755–67. [https://doi.org/10.1016/S1359-6454\(98\)00226-2](https://doi.org/10.1016/S1359-6454(98)00226-2).

- [21] Lu Z, Feng Y, Peng G, Yang R, Huan Y, Zhang T. Estimation of surface equi-biaxial residual stress by using instrumented sharp indentation. *Mater Sci Eng, A* 2014; 614:264–72. <https://doi.org/10.1016/j.msea.2014.07.041>.
- [22] Wang Q, Ozaki K, Ishikawa H, Nakano S, Ogiso H. Indentation method to measure the residual stress induced by ion implantation. *Nucl Instrum Methods Phys Res B* 2006;242:88–92. <https://doi.org/10.1016/j.nimb.2005.08.008>.
- [23] Lee Y-H, Kwon D. Estimation of biaxial surface stress by instrumented indentation with sharp indenters. *Acta Mater* 2004;52:1555–63. <https://doi.org/10.1016/j.actamat.2003.12.006>.
- [24] Rahimian Koloor S, Karimzadeh A, Tamin M, Abd Shukor M. Effects of sample and indenter configurations of nanoindentation experiment on the mechanical behavior and properties of ductile materials. *Metals* 2018;8:421. <https://doi.org/10.3390/met8060421>.
- [25] Celentano DJ, Guelorget B, François M, Cruchaga MA, Slimane A. Numerical simulation and experimental validation of the microindentation test applied to bulk elastoplastic materials. *Model Simulat Mater Sci Eng* 2012;20:045007. <https://doi.org/10.1088/0965-0393/20/4/045007>.
- [26] Everaerts J, Salvati E, Korsunsky AM. Nanoscale depth profiling of residual stresses due to fine surface finishing. *Adv Mater Interfac* 2019;6:1–5. <https://doi.org/10.1002/admi.201900947>.
- [27] NPL - Measurement Good Practice Guide N. Determination of residual stresses by X-ray diffraction, vol. 52; 2005.
- [28] Montross CS, Wei T, Ye L, Clark G, Mai YW. Laser shock processing and its effects on microstructure and properties of metal alloys: a review. *Int J Fatig* 2002;24: 1021–36. [https://doi.org/10.1016/S0142-1123\(02\)00022-1](https://doi.org/10.1016/S0142-1123(02)00022-1).
- [29] Mostafa AM, Hameed MF, Obayya SS. Effect of laser shock peening on the hardness of AL-7075 alloy. *J King Saud Univ Sci* 2019;31:472–8. <https://doi.org/10.1016/j.jksus.2017.07.012>.
- [30] Thiruneelakandan R, Balamurugan R, Prakasam R. Improved surface property of Al-7075 alloy by laser shock peening technique. *Mater Today Proc* 2023;92: 1597–601. <https://doi.org/10.1016/j.matpr.2023.06.087>.
- [31] Zhang Z, Yang Y, Gao Y, Wang G, Shi W. Performance analysis of 7075 aluminum alloy strengthened by cavitation water jet peening at different scanning speeds. *Crystals* 2022;12. <https://doi.org/10.3390/cryst12101451>.
- [32] Ding K, Ye L. Physical and mechanical mechanisms of laser shock peening. In: Ding K, Ye L, editors. *Laser shock peen*. Elsevier, Woodhead Publishing; 2006. p. 7–46. <https://doi.org/10.1533/9781845691097.7>.
- [33] Attolico MA, Barile C, Casavola C, Moramarco V, Furfari D, Busse DO. Effects of laser shock peening on surface roughness and residual stress of AA 7050-T7451. *J Mater Eng Perform* 2022;31:7973–88. <https://doi.org/10.1007/s11665-022-06857-7>.